



# Strainburst characteristics under bolt support conditions: an experimental study

Xiaochuan Hu<sup>1</sup> · Guoshao Su<sup>1,2,3</sup> · Kang Chen<sup>1</sup> · Tianbin Li<sup>2</sup> · Quan Jiang<sup>3</sup>

Received: 8 November 2018 / Accepted: 17 July 2019 / Published online: 22 July 2019  
© Springer Nature B.V. 2019

## Abstract

Strainburst, defined as a burst that occurs on the periphery of tunnels, is always associated with intact and hard brittle rocks and high geo-stress. In practical engineering, the prevention of strainburst by bolting does not achieve the desired effects. Deep insight into the strainburst process and mechanisms under bolt support conditions is necessary to ensure safe underground construction. In this study, strainburst characteristics under bolt support conditions were investigated using a true-triaxial rockburst testing system, which was equipped with an acoustic emission monitoring system. High-speed cameras were also used to capture the ejection failure process. Two indicators, namely kinetic energy and maximum decibel, were used to comprehensively evaluate the rockburst intensity. In addition, characteristic stresses, failure mode and cracking mechanisms under different bolt spacing conditions were investigated. The test results demonstrated that rockburst is greatly affected by the bolt arrangement. Rockburst changes from the way occurring in the form of a local failure in weak area to the way striking the bolt position and even the overall free face with the decrease in bolt spacing. The use of the bolt increases the rockburst intensity, but the intensity decreases as the bolt spacing decreases. Characteristic stresses including crack initiation stress, crack damage stress and peak strength increase monotonously with the use of bolt and the decreasing bolt spacing. During the strainburst, tensile failure dominates the cracking process regardless of bolt spacing; however, with the use of bolt and decrease in bolt spacing, tensile splitting near the free face become less obvious and the proportion of shear failure gradually increased.

**Keywords** Rockburst · Strainburst · Bolt support · True-triaxial tests

---

✉ Guoshao Su  
guoshaosu@gxu.edu.cn

<sup>1</sup> Key Laboratory of Disaster Prevention and Structural Safety of Ministry of Education, School of Civil and Architecture Engineering, Guangxi University, Nanning 530004, People's Republic of China

<sup>2</sup> State Key Laboratory of Geohazard Prevention and Geoenvironment Protection, Chengdu 610059, People's Republic of China

<sup>3</sup> State Key Laboratory of Geomechanics and Geotechnical Engineering, Institute of Rock and Soil Mechanics, Chinese Academy of Sciences, Wuhan 430071, People's Republic of China

## 1 Introduction

In deep excavations of hard rock, the failure process is often governed by the mechanism of stress-induced brittle failure (Kaiser et al. 2000). When excavation-induced stress reaches the strength of the rock mass, rockburst may occur in an unstable or violent manner, leading to a sudden damage of the excavation periphery with an explosive release of elastic strain energy and fragments ejection (Cook et al. 1966; Hedley 1992; Kaiser 1996; Zhang et al. 2013; Gao et al. 2019; Gong et al. 2019). Because of its great danger, rockburst posed great safety risk and economic loss (Wang et al. 2012; Zhang et al. 2012; Feng et al. 2013). For example, an extremely intense rockburst struck the drainage of the Jinping II Hydropower Station in China on November 28, 2009, leading to destruction of a tunnel-boring machine (TBM) and seven deaths. As the excavation depth increases, this violent failure will become increasingly intense and pervasive due to high geo-stress.

Extensive studies (Cook 1965; Cook et al. 1966; Salamon 1970; Kaiser and Cai 2012; Zhang et al. 2014; Zhao and Cai 2014; Gong et al. 2018), including theory analyses, numerical simulations, field investigations and physical tests, have been performed to elucidate the mechanism and development of rockburst since the early works on this topic (Cook 1963). For example, Salamon (1970) discussed the role between loading machine stiffness ( $k$ ) and post-peak stiffness ( $\lambda$ ) of specimen in unstable failure and noted that when the stiffness condition  $k + \lambda$  is negative definite, the unstable failure or rock burst will occur. As it is one of the most common rockburst types, strainburst has received more attention. Kaiser and Cai (2012) thought tangential stress concentration and a relatively soft loading environment are the two necessary factors to trigger the strainburst; Zhao and Cai (2014) investigated the influence of height-to-width ratio on strainburst characteristics; Gong et al. (2018) conducted experimental simulation investigation on rockburst induced by spalling failure in deep circular tunnels. However, because of its complex characteristics, strainburst hazard is far from satisfactorily addressed. Hence, a good understanding of strainburst (hereinafter referred to as rockburst) is very important.

So far, various approaches, such as changing the project layout scheme and excavation method, optimizing the excavation shape, dimensions and sequences and utilizing acoustic emission (AE) and microseismic (MS) technology, were used to reduce the potential rockburst risk or help to maintain stability of the surrounding rock mass during deep excavations (Tang et al. 2010; Feng et al. 2016). However, the key factor to preventing the rockburst is still through rock mass supports. Among these supporting methods, bolt support is one of the most basic and practical approaches and has been widely used in deep excavation. However, after bolt reinforcement of hard brittle rock mass, the surface parallel micro-crack or onion-skin fractures and even rockbursts are still frequent as the tunnel face advances. The method of rockburst control by bolting does not achieve the desired results (Fig. 1). For example, on July 16, 2011, an intense rockburst occurred at SK7+255–7+259 in diversion tunnel #4 in the Jinping II Hydropower Station, resulting in a V-shaped rockburst notch with a maximum depth of 0.8 m, serious damages to the support systems and a number of bolts being exposed to air (Feng et al. 2013). Due to the lack of effective real-time monitoring methods and in-depth investigations of in situ rockbursts, our understanding of the rockburst process and mechanism under bolt support conditions lags behind the engineering practice of deep hard brittle rock mass. As a result, even if considerable effort has been made in terms of support strategy, high-performance bolt and related physical test studies, the prevention of rockbursts by bolts is still very problematic.

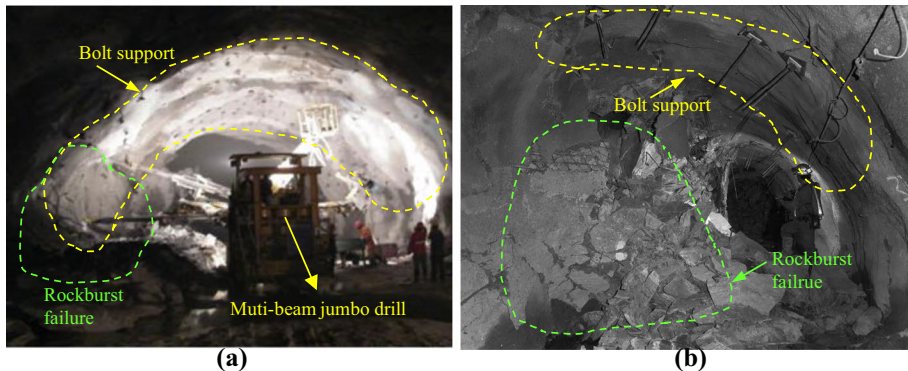


**Fig. 1** Rockburst under bolt support at the: **a** Jinping II Hydropower Station in China (Zhang et al. 2012); **b** East Rand Proprietary Mines in South Africa (Ortlepp 2000)

Rockburst process and mechanism investigations based on laboratory tests are the core of rockburst studies. Based on laboratory physical tests, considerable studies have been conducted (Cook 1965; Ortlepp and Stacey 1994; He et al. 2012). Physical tests have developed from uniaxial tests (Cook 1963; Singh 1987), to biaxial tests (Zuo et al. 2006; Zhang 2011) and to pseudo-triaxial tests (Hua and You 2001; Chen et al. 2009). In recent years, with the development of more advanced experimental instruments, true-triaxial rockburst tests (He et al. 2010; Gong et al. 2015) are becoming a trend, making it possible to observe the ejection process of fragments from a free surface after rockburst. It realized an effective simulation for the transformations of the stress state and boundary conditions of rock mass at or near the excavation boundary and may be comparable with in situ rockburst in terms of fracturing process and violent fragment ejection. For example, Zhao et al. (2014) investigated the influence of unloading rate on the strainburst characteristics of Beishan granite. Su et al. (2017b) carried out a series of tests to investigate the influence of radial stress gradient on strainburst and revealed that the strength increases with an increasing radial stress gradient. However, the failure process and mechanisms of rockburst under bolting remain unclear and also have not been studied systematically. Therefore, it warrants more investigations to eliminate and mitigate rockburst hazards to reduce property damage and ensure workers' safety.

This paper aims to investigate the rockburst characteristics under the condition of bolt support with high-speed cameras and acoustic emission (AE) monitoring system. In the following studies, true-triaxial rockburst testing system is first introduced. Then, rockburst testing, including specimen preparation and stress state and stress path, is described. Finally, testing results, including ejection process, rockburst intensity, characteristic stresses, and failure mode and cracking mechanisms, are investigated in detail.

## 2 True-triaxial rockburst testing system

The true-triaxial rockburst testing system, developed at Guangxi University, Nanning, China, was used to conduct the rockburst tests. The testing system mainly consists of rockburst test machine, AE monitoring system and two high-speed cameras (Fig. 2a). The rockburst test machine can load/unload in three mutually orthogonal directions and provide maximum

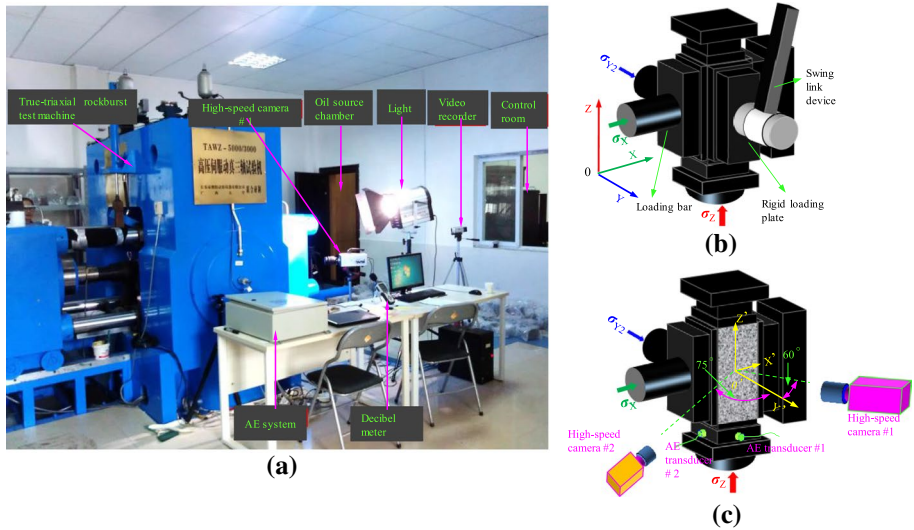


**Fig. 2** True-triaxial testing system: **a** full view; **b** loading devices for unloading stress path; **c** loading method used in the present study

loads of 5000 kN and 3500 kN in the vertical direction ( $Z$  direction) and horizontal directions ( $X$  direction and  $Y$  direction), respectively. The stiffness of the vertical frame is greater than 9000 kN/mm, and those of the horizontal frames are greater than 5000 kN/mm. Due to its two mutually independent loading systems in the  $Y$  direction, load in the  $Y$  direction can be abruptly unloaded on one face using a rotating swing link device (Fig. 2b), while the loads on other faces are maintained, leading to a special unloading stress path (loading on six faces and then unloading on single face). In addition, another stress path, leaving one face free and loading on the other five faces, can be realized to simulate excavation-induced stress concentration (Fig. 2c), leading to a loading stress path. Additionally, this testing system can be used to perform uniaxial, biaxial, and true-triaxial compression tests.

Two high-speed cameras, GVCM08-B05 and IM-VG03-1-117B, were used to monitor the macroscopic fracturing and ejection failure process (Fig. 3a), and its layout is presented in Fig. 2c. The recording speed of the both two high-speed cameras was set to 500 fps. In the present study, two AE transducers with a diameter of 18 mm were utilized to capture the AE characteristics of the rock specimen during the loading process. The AE transducers have a resonant frequency of 103 kHz and a sampling rate of 1 MSPS, and the AE trigger threshold was set to 40 dB. Two AE transducers were attached to the surfaces of the base instead of in direct contact with the rock specimen (Fig. 2c). To reduce the signal attenuation, a small amount of butter was applied to the interfaces between the base and the transducers. In addition, recording pen and decibel meter were placed near the specimen to record the sound from failure (Fig. 3c).

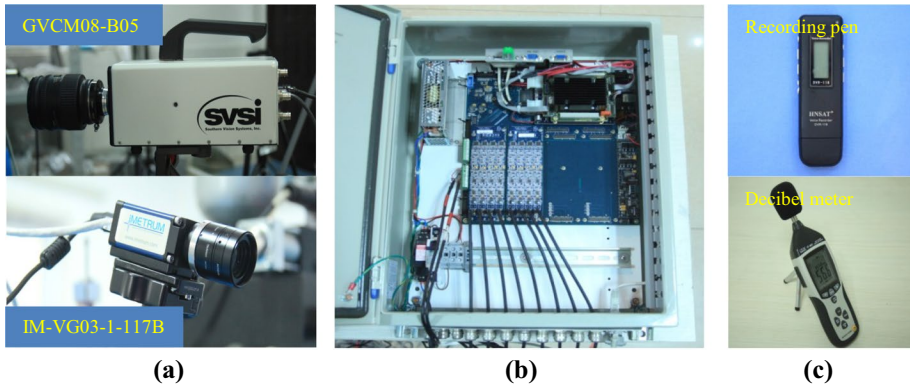


**Fig. 3** Monitoring system: **a** high-speed cameras; **b** AE system; **c** recording pen and decibel meter

### 3 Testing

#### 3.1 Specimen preparation

The specimens for tests were cut from intact, white coarse-grained granite, a typical hard brittle rock material from Guangxi Province, China. Figure 4 shows the naked-eye observation, three-dimensional hyper-focal distance microscopic image, and the optical cross-polarized micrograph of the tested rocks. A quantitative mineralogical composition analysis showed that the rock is mainly comprised of approximately 39% plagioclase, 28% quartz, 18% potash feldspar, 7% biotite and 3% hornblende; the size of these mineral grains mainly ranges from 0.6 to 5.5 mm. Table 1 presents the basic properties for this kind of granite material. Before true-triaxial rockburst tests, the rectangular prismatic specimens, 100 mm × 100 mm × 200 mm, were prepared, and all sides and ends of the specimens were finely ground and polished to minimize the local stress concentration.

In order to investigate the rockburst characteristics under different bolting conditions, different number and arrangement of boreholes were carefully drilled into the rock

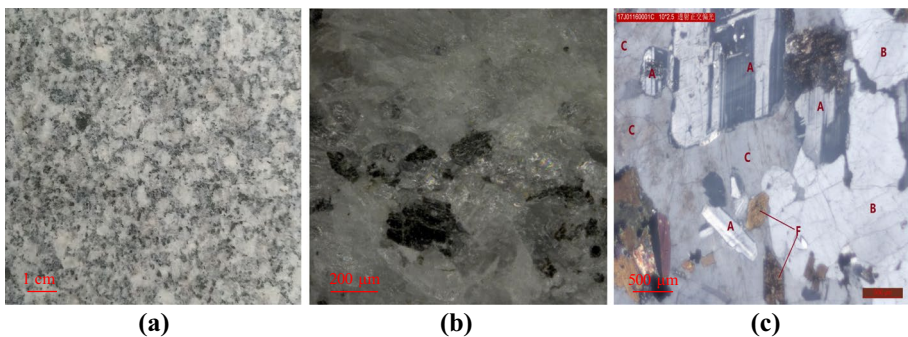


**Fig. 4** Geological nature of granite at different scales: **a** naked-eye observation; **b** 3D microscope observation; **c** optical cross-polarized observation (A, B and C in **c** denote plagioclase, quartz and potash feldspar, respectively)

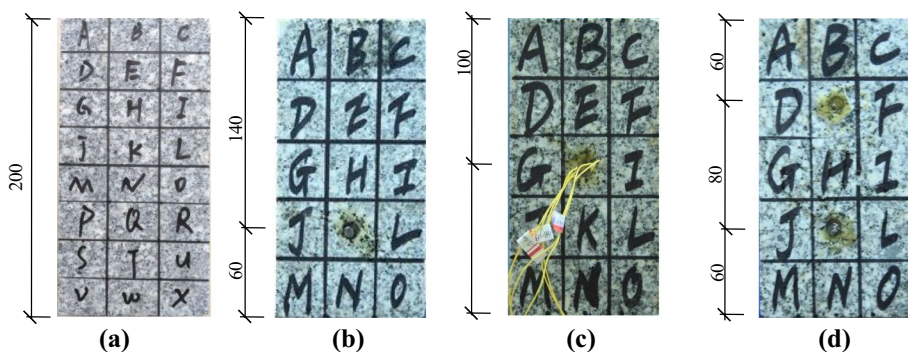
**Table 1** Basic properties of the granite material

Rock type	Density (g/cm <sup>3</sup> )	UCS (MPa)	Young's modulus (GPa)	Poisson's ratio	P-wave velocity (km/s)
Granite	2.64	165	34.3	0.26	5.4

specimen. Borehole has a diameter of 8 mm and a depth of 75 mm. The bolt has a diameter of 6 mm, and its yield limit is approximately 235 MPa. After installing the bolt, the borehole was grouted with epoxy resin so that the bolt and rock material are well bonded. Four different bolt support conditions are shown in Fig. 5, and two specimens for each condition were prepared to conduct the test. After bolting, the maximum spacing, ranging from 140 to 80 mm (Fig. 5b–d), is defined as bolt spacing. In addition, one face, called the free face in the following sections, of the specimen was divided into several subregions to better capture the ejection failure process.

### 3.2 Stress state and stress path

The stress state in space is defined by three mutually perpendicular principal stress components ( $\sigma_1, \sigma_2, \sigma_3$ ). On the boundary, a state of biaxial stress,  $\sigma_1 \neq 0, \sigma_2 \neq 0$  and  $\sigma_3 = 0$ , exists, and away from excavation boundary, the rock mass is in a true-triaxial stress state where  $\sigma_1 > \sigma_2 > \sigma_3$  (Fig. 6). In fact, rockburst is a structural dynamic failure rather than a simple material failure. As a result, a representative rock element was devised to describe the complex stress state of rock mass near the excavation boundary within a certain depth (Fig. 6). Stress state of five surfaces loaded with one face free exists for the representative rock element because the opening boundary was exposed to air after excavation. Due to the constraints from the remaining surrounding rock mass, shear stress also exists on the surface of the representative rock element (Fig. 6); this shear stress can be simulated realistically with friction at the interface between the end of the rock specimen and loading plate (Fig. 2c). Therefore, representative rock element in our present study was in a non-principal stress space, rather than in the principal stress space, in which most previous laboratory tests were conducted to explore the mechanical properties of rocks.

**Fig. 5** Four different bolt support conditions. Unit: mm

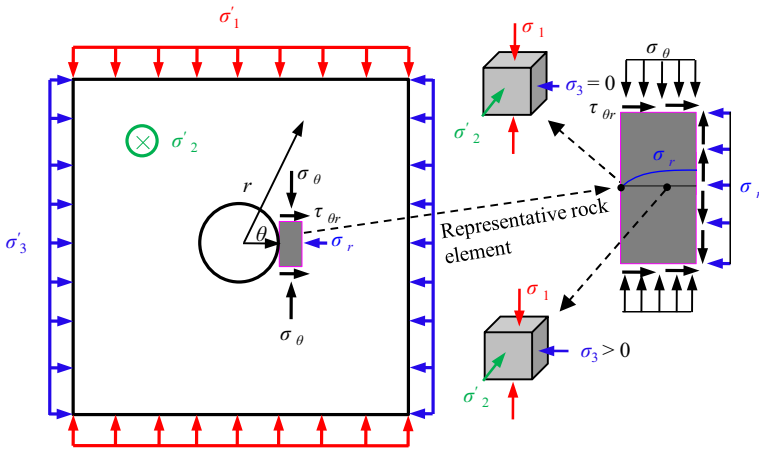


**Fig. 6** Stress state after excavation.  $\sigma'_1$  and  $\sigma'_3$  are the major and minor in situ (far-field) principal stresses, respectively;  $\sigma'_2$  is the intermediate principal stress (in the direction of the opening axis);  $\sigma_\theta$  and  $\tau_{\theta r}$  are the tangential and radial stresses, respectively;  $r$  is the radial distance from the axis of the opening; and  $\theta$  is the azimuth angle measured counterclockwise from the  $\sigma'_3$  direction

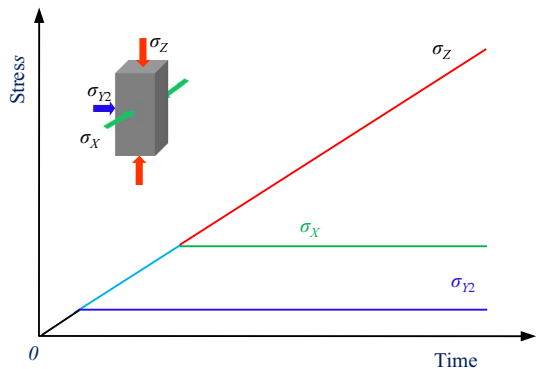
As tunnel face advances, the tangential stress  $\sigma_\theta$  of rock mass at or near the excavation continues to build up until plane strain condition is approximately obtained. When  $\sigma_\theta$  reaches the strength of the rock mass, the surplus strain energy after fracturing would be released in a violent manner, resulting in the occurrence of rockburst. Consequently, a continuous loading stress path or loading rockburst (Su et al. 2017a) may be more suitable for reproducing the in situ failure process. The stress path, maintaining one free face while loading on the other five faces until the occurrence of rockburst, is presented in Fig. 7 and described as follows:

*Step 1* The loads on five faces are increased at a constant loading rate until the predetermined magnitude of 5 MPa is reached.

*Step 2*  $\sigma_x$  and  $\sigma_z$  are raised simultaneously until the preset magnitude of 30 MPa is reached, while  $\sigma_{y2}$  is maintained constant.

*Step 3*  $\sigma_z$  is increased until the occurrence of rockburst, while the loads on the other three faces are maintained to be constant.

**Fig. 7** Stress path



During the test, a free face in the *Y* direction is always maintained, and the loading rate of 0.5 MPa/s (strain rate: approximately  $1.5 \times 10^{-5} \text{ s}^{-1}$ ) is adopted.

## 4 Testing results

### 4.1 Influence of bolt on ejection failure

The ejection failure process of each specimen was captured using two high-speed cameras recording in different directions (Fig. 2c), and a series of key snapshots recorded by high-speed camera #1 were used to illustrate the rockburst (Fig. 8). Note that the high-speed camera #2 is auxiliary and used to verify the speed and kinetic energy evaluated with video captured by high-speed camera #1 in the following section. In the initial stage, particle ejection first occurred on the free face due to the heterogeneity and stress concentration. With a further stress concentration, macroscopic splitting failure occurred near free face, resulting in several tensile fractures subparallel to the free face. These tensile fractures continued to bend and store strain energy until buckling to the point of rupture, and the surplus energy after fracturing was released in the form of kinetic energy of ejected fragments. As a result, all specimens underwent a similar rockburst failure process, i.e., grains ejection, splitting into plates, buckling to the point of rupture and fragments ejection (Fig. 8).

However, it can be seen that the bolt significantly affects the ejection process and failure characteristics of the rockburst. Figure 9 presents the rockburst pits after the test. It can be found in Figs. 8 and 9 that tension-induced rock flakes are always broken near the bolt, suggesting that the bolt restrains the development of tensile fractures. Compared with failure process and result without bolt (e.g., specimen M1), the rockburst always occurs in the form of a local failure when bolt spacing is 140 and 100 mm (Fig. 9b–e). The failure will be limited to a local area and will not pass through the bolt. In this case, there is a large weak area left after the bolt support, so the rockburst always occurs in the weak area (e.g., the lower section of specimen M3 and the upper section of the specimen M7), and the area with strong support (e.g., the upper section of specimen M3 and the lower section of specimen M4) will not suffer from macroscopic damage and are relatively complete. However, when the bolt spacing is smaller or bolt support is stronger (e.g., 80 mm for specimens M7 and M8), the blank area after the bolt support is smaller and the bearing capacity of each part of the test specimen is almost equal, indicating that is no obvious weak area. Under this case, the failure will not be constrained in the weak area and will pass through the bolt and even occur throughout the free face (specimens M7 and M8 in Fig. 9). Therefore, the ejection failure is obviously affected by the bolt support and changes with the bolt spacing.

In addition, the maximum depth of the failure zone and the mass of ejected fragments are greatly affected by the bolt. When no bolt was used, the maximum depth is 3.2 mm, and it decreases to 0.98 mm as bolt spacing decreases to 80 mm (Table 2). The mass of ejected fragments also experiences a similar decreasing trend (from 415.71 to 202.52 g). Therefore, the use of the bolt reduces maximum depth of rockburst pit and the mass of the ejected fragments, and they also continue to decrease as the bolt spacing decreases.

### 4.2 Influence of bolt on rockburst intensity

Rockburst intensity is an important indicator for evaluating failure severity and an important part of rockburst studies. In the present study, three indicators, including kinetic



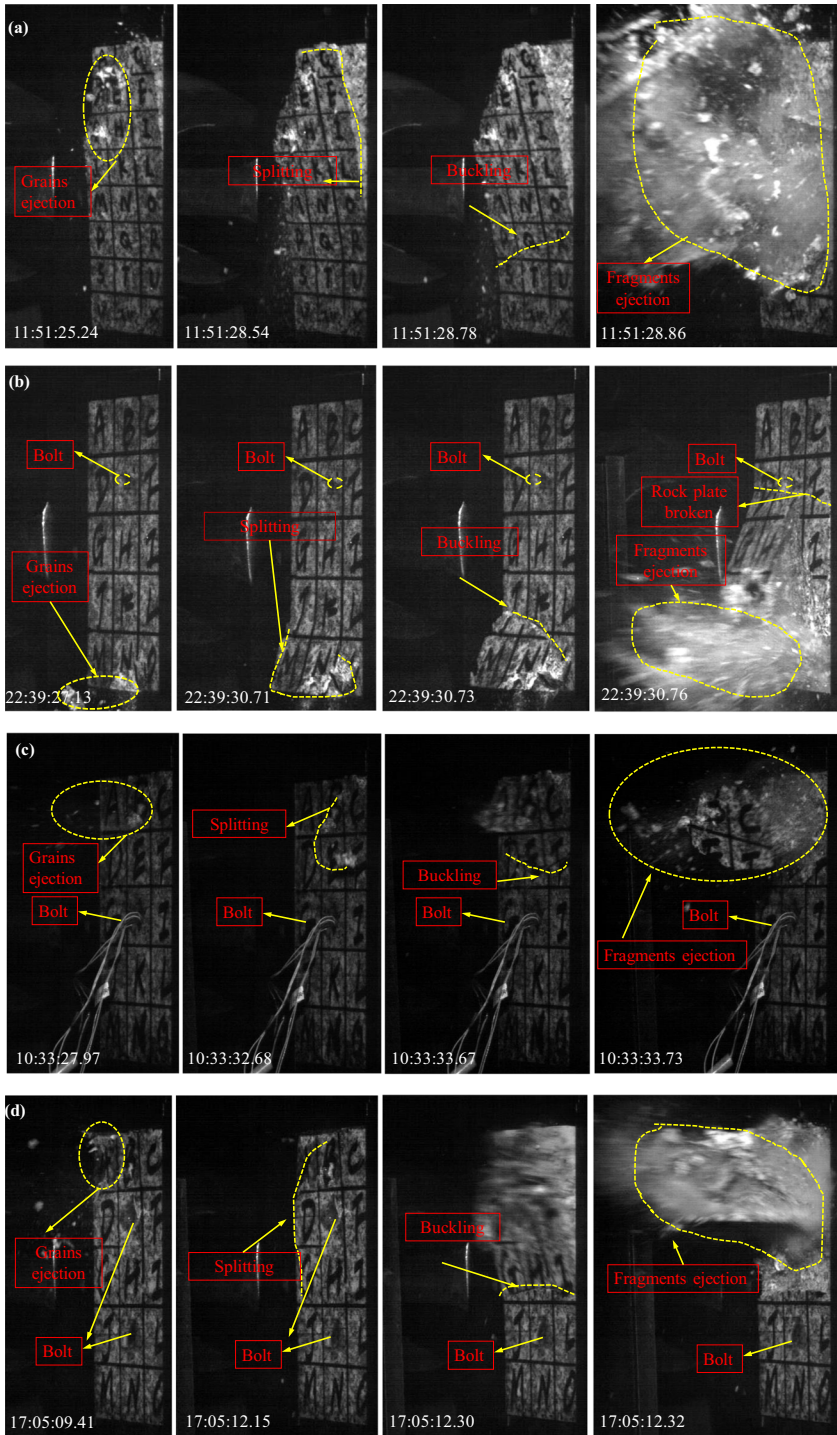


**Fig. 8** Typical failure process captured by high-speed camera #1: **a** M1; **b** M3; **c** M5; **d** M8 (the numbers at the bottom-left corner of the pictures indicate the time in h:m:s)

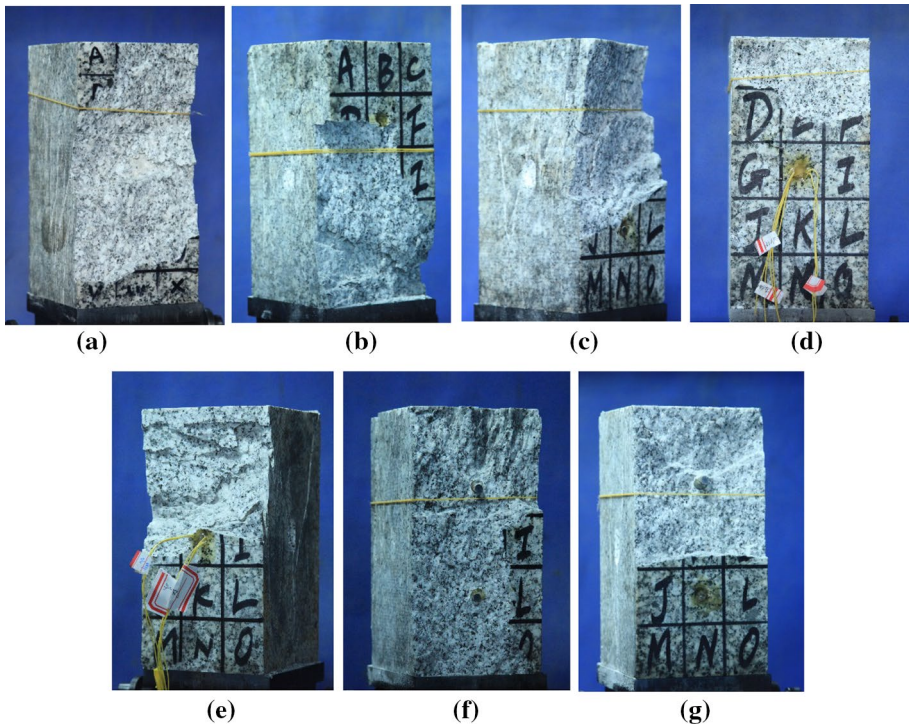


**Fig. 9** Rockburst pits: **a** M1; **b** M3; **c** M4; **d** M5; **e** M6; **f** M7; **g**: M8. Note that strain gauges used to monitor the strain of the bolt for specimens M5 and M6 have failed during the test

**Table 2** Test results

Sample no.	Dimension of rockburst pit (cm × cm × cm)	Mass of ejected fragments (g)	Kinetic energy (J)	Cumulative AE energy ( $10^9$ aJ)	Maximum decibel (dB)	Maximum spacing (mm)
M1	18.0 × 10.0 × 3.2	415.71	2.40	2.92	98.4	–
M2	–	–	–	–	–	–
M3	14.0 × 10.0 × 2.5	328.42	4.69	4.65	106.3	140
M4	14.0 × 10.0 × 2.2	366.21	5.26	3.54	110.9	140
M5	5.9 × 10.0 × 1.6	–	–	2.91	96.4	100
M6	10.6 × 10.0 × 3.3	–	3.00	3.2	101.5	100
M7	20.0 × 10.0 × 0.98	–	–	2.75	86.8	80
M8	12.0 × 10.0 × 1.4	202.52	2.37	3.11	86.3	80

– Information has not been effectively collected. Dimension indicates the height, width and maximum depth of the pit, respectively. Maximum spacing is defined as bolt spacing in the present study

energy, cumulative AE energy, and maximum decibel, were used to comprehensively evaluate the rockburst intensity.

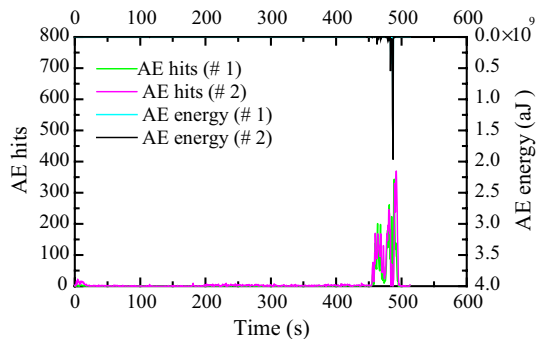
Kinetic energy of the ejected fragments, considered one of the most direct indicators for the quantitative analyses of rockburst failure, has also been adopted to assess the rockburst intensity (Su et al. 2017b). In the present study, the kinetic energy of the ejected fragments was measured and evaluated for each specimen. The specific assessment methods refer to Su et al. (2017b), and the results are presented in Table 2. As observed, the use of the bolt significantly changes the kinetic energy of the fragments. For example, the kinetic energies of M3 and M4 are 4.69 J and 5.26 J, respectively, increasing 95.4% and 119.2% compared with specimen M1. The use of the bolt increases the strength so that more elastic strain energy can be released, meaning more kinetic energy. Increase in kinetic energy suggests that once the rock mass under the support is subjected to rockburst, it will cause more serious damage. However, the energy decreases with the decreasing bolt spacing. For example, it decreases from 4.69 to 2.37 J when bolt spacing decreases from 140 to 80 mm. As the bolt spacing continues to decrease, the mass of the ejected fragments has been significantly reduced, thus resulting in a reduction in kinetic energy.

In addition, cumulative AE energy and maximum decibel during the failure process experienced an evolution trend consistent with that of kinetic energy and reach the maximum when the bolt spacing is 140 mm. In previous studies, maximum decibel was successfully used for rockburst intensity assessment (Su et al. 2017a). However, whether the cumulative AE energy, one of the indicators for evaluating the energy released by cracking, is suitable to evaluate the rockburst intensity requires further research. In summary, two indicators, namely kinetic energy and maximum decibel, reveal that rockburst intensity increases with the use of bolt support, but decreases with the decreasing bolt spacing under the bolt support condition.

### 4.3 Influence of bolt on characteristic stresses

The cracking event in rock material is accompanied by the release of strain energy, and its resulting elastic wave can be captured with AE system. Consequently, AE signal can be used to reflect the cracking activity in the rock material. Figure 10 presents the AE hits and energy captured during the test for specimen M1. As observed, the trend and magnitude of AE activity are similar, indicating that the AE signals captured by both transducers can well reflect the internal cracking activity. In the present study, AE signals captured by

**Fig. 10** AE hits and energy of two transducers during the test for specimen M1



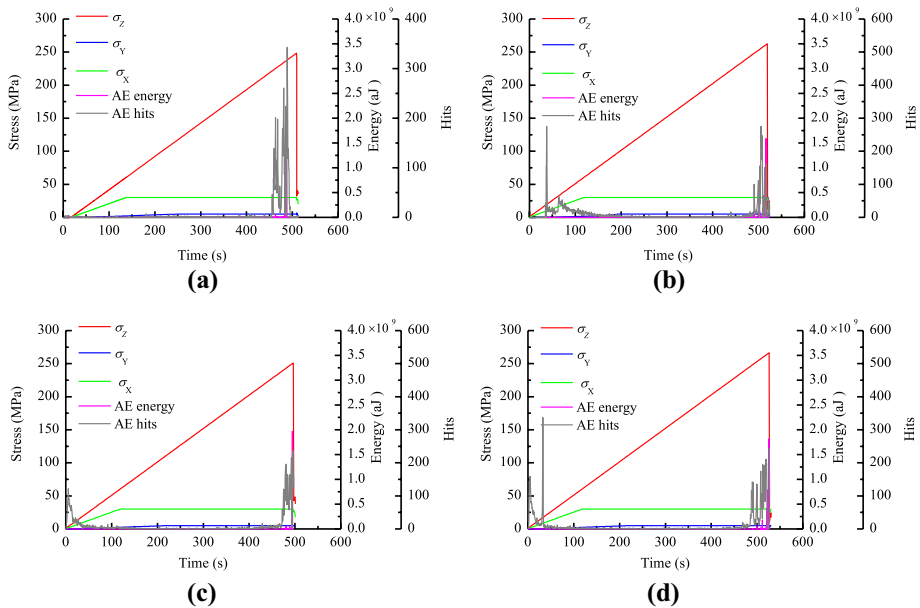


**Fig. 11** Stress paths and AE responses for the tested specimens: **a** M1; **b** M3; **c** M5; **d** M8

transducer #1 were used for further studies. Due to space limitation, only some AE results are given in Fig. 11.

Crack initiation stress  $\sigma_{ci}$  represents the dilatancy onset or initiation of microscopic cracks, and it usually occurs at stress level of 0.3–0.5 UCS under uniaxial compression. It plays an important role in assessing the in situ spalling strength and quantifying the failure process of intact rock specimen (Martin and Chandler 1994; Cai and Kaiser 2014). However, the methods under different conditions, especially for complex loading conditions and specimen geometry, are not the same, and there are no uniform standards to use. For example, Weng et al. (2018) considered the value equal to the stress level when the first tensile crack is triggered in the opening as the crack initiation stress; Zhu et al. (2015) took the axial stress when the inner wall started caving in as the initiation stress for specimens with two circular holes; Cheon et al. (2011) determined the failure initiation stress of a physical model specimen as the point at which cumulative AE hits start to increase significantly for the first time, and the results are consistent with in situ investigation (Martin 1997). Therefore, the method adopted by Cheon et al. (2011) was used to determine the crack initiation stress in this study. Further, crack damage threshold can also be determined referring to Cheon et al. (2011).

Figure 12 gives an example for determining the crack initiation stress  $\sigma_{ci}$  and crack damage threshold  $\sigma_{cd}$ , and these characteristic stresses for other specimens are also presented in Table 3. As observed,  $\sigma_{ci}$  increases with the use of bolt and also continues to increase with the decreasing bolt spacing. For example, when no bolt was used (e.g., specimen M1), the crack initiation stress is 93.9 MPa. However,  $\sigma_{ci}$  increases to 136.9 MPa when bolt spacing decreases to 80 mm (e.g., specimen M8). Consequently, bolts play a similar role with confining pressure, because extensive studies have indicated that  $\sigma_{ci}$  increases with an increasing confining pressure (Diederichs 2007). In addition, it is generally realized that tensile cracks dominated the microscopic fracturing process until unstable development of cracks

**Fig. 12** Determination of damage thresholds during the test for specimen M4

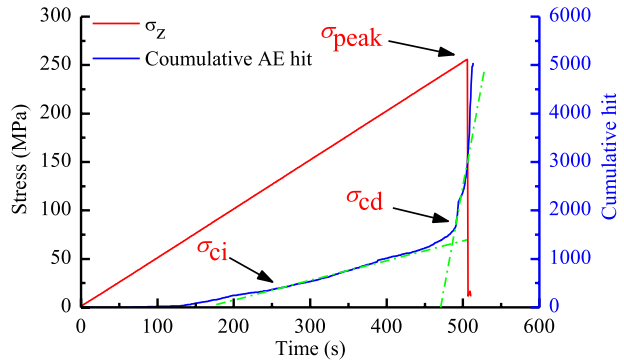


**Table 3** Characteristic stresses

Sample no.	M1	M2	M3	M4	M5	M6	M7	M8
$\sigma_{ci}$	93.9	–	101.4	106.4	100.2	102.5	–	136.9
$\sigma_{cd}$	218	–	248	243.2	238.2	248.2	–	241.9
$\sigma_{peak}$	245	–	262	256	250.8	265	–	270
$\sigma_{ci}/\sigma_{peak}$	0.38	–	0.39	0.42	0.40	0.39	–	0.51
$\sigma_{cd}/\sigma_{peak}$	0.89	–	0.95	0.95	0.95	0.94	–	0.90

Note that the loading process was not captured for specimens M2 and M7, and only some failure results are available

(Brace et al. 1966; Lajtai et al. 1990). Therefore, the use of bolt and the decreasing bolt spacing retard the occurrence or initiation of tensile crack and then the crack damage stress  $\sigma_{cd}$  and peak stress  $\sigma_{peak}$  (Table 3).

The ratios of  $\sigma_{ci}$  and  $\sigma_{cd}$  to  $\sigma_{peak}$  were also calculated. As presented in Table 3, the ratio of  $\sigma_{ci}/\sigma_{peak}$  is in the range of 0.38–0.51. However, the ratio of  $\sigma_{cd}/\sigma_{peak}$  seems to be at a very high level (can be as high as 0.95). Under the true-triaxial compression tests for KTB amphibolite (Chang and Haimson 2000), a relatively high  $\sigma_{cd}/\sigma_{peak}$  was also observed, indicating that it may be related to stress state. Therefore, the results about  $\sigma_{ci}$  and  $\sigma_{cd}$  are reliable.

## 4.4 Influence of bolt on failure mode and cracking mechanism

### 4.4.1 Macroscopic failure mode

The rock away from the free face is generally in a true-triaxial stress state; consequently, macroscopic shear fracture or fault can be observed away from the free face in all specimens (Fig. 13). A large amount of gray-white powder was found between these shear faults (Fig. 14), indicating that a strong friction has occurred during the fracturing process. The rock at or near the stress-free face is subjected to a higher vertical compressive stress and a zero or lower confining stress, similar to uniaxial stress state or triaxial compressive stress state under low confining stress; as a result, several tensile fractures subparallel to the free face can be clearly observed (Fig. 13). Finding that the micro-cracks within ejected fragments were subparallel to vertical stress direction (Fig. 14) also suggests the tensile failure occurred near the free face. As a result, all failure presents a similar zoning mode, i.e.,

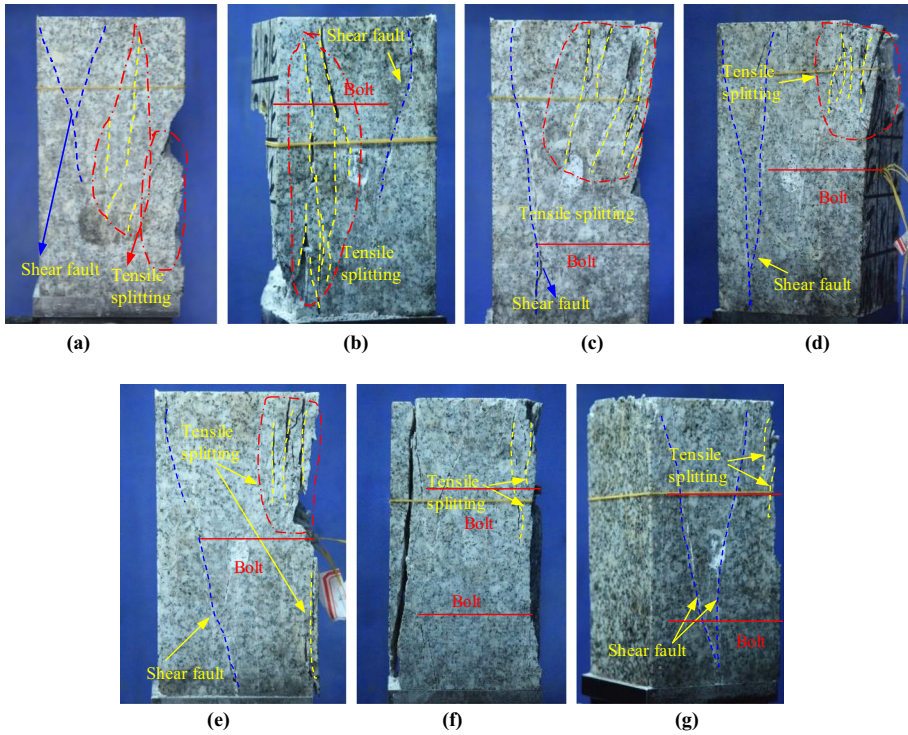


**Fig. 13** Fracturing results of the tested specimens: **a** M1; **b** M3; **c** M4; **d** M5; **e** M6; **f** M7; **g** M8

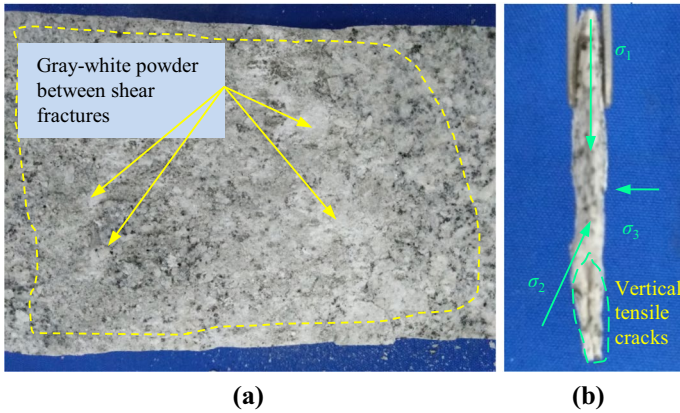


**Fig. 14** **a** Gray-white powder between the shear faults; **b** tensile cracking parallel to vertical stress

rockburst pit at the free face, tensile splitting near the free face and shear fracturing away from the free face.

In fact, the severity of tensile splitting near the free face is greatly affected by bolt. As observed in Fig. 13, the tensile fractures are especially dense when no bolt is used

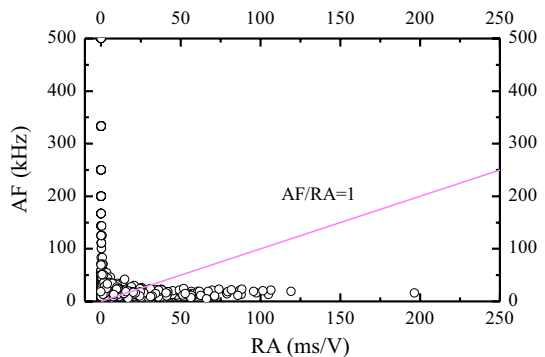
(Fig. 13a). When the bolt spacing is 140 or 100 mm, only few macroscopic tensile fractures can be observed, and the thickness of splitting-induced flake increases significantly (Fig. 13b–e). When bolt spacing is 80 mm, the tensile splitting becomes less obvious, and only one or two splitting fractures can be observed near the free face (Fig. 13f, g). In general, the generation of micro-cracks is related to the confining pressure, and the length of micro-crack is proportional to the deviatoric stress, and more restriction or higher confining pressure due to bolt makes the cracks less easy to initiate and develop. Therefore, with the use of bolt and the decreasing bolts spacing, the tensile splitting near the free surface decreases, and the density or number of tensile fractures reduces. However, shear fractures appear to be unaffected from a macro-perspective, and it always dominates the failure away from the free face in the form of one or two faults. According to considerable in situ investigations and observations, tensile splitting dominates the crystalline rocks near the excavation boundary (Diederichs 2007; Martin and Christiansson 2009). Further, splitting is the pioneer or precursor of rockburst, and it is inevitable for rockburst occurrence. Consequently, rockburst can be prevented by appropriately increasing the bolt density.

#### 4.4.2 Cracking mechanism

Generally, three types of micro-cracks, Mode I—tensile crack, Mode II—shear crack, and Mode III—combination of the two, exist during the cracking of rock material. According to Aggelis (2011), crack initiation and propagation incidents have different AE signal characteristics depending on the cracking types. Thus, this difference can be used to identify the cracking types or cracking mechanisms. In the present study, the ratio of AF (the average frequency value = AE ring-down count/the duration time) to RA (the rise angle value = the rise time/the maximum amplitude) of the AE signal was used to quantitatively investigate the cracking mechanism, i.e., a crack was produced by tensile cracking if this ratio is larger than a given value; otherwise, it derived from shear cracking. It should be noted that only two kinds of cracks, Mode I and Mode II, were assumed. AF/RA has been used to identify different cracking modes in concrete material (Aggelis 2011; Shahidan et al. 2013); however, its applications in rock material are rare, especially in quantitative elucidation of cracking mechanisms. For more details about the AF and RA, readers can refer to Grosse and Ohtsu (2008).

In order to confirm the ratio of AF/RA, three-point bending test was conducted with the same rock material, and the AF and RA values of the AE signals during the test were obtained (Fig. 15). Consequently, the ratio of 1 was used to differentiate the cracking

**Fig. 15** AF and RA characteristics of AE hits during the three-point bending test



modes (Fig. 15); under this conditions, approximately 78% of the AE signals derived from tensile cracks. As an approximation, it is assumed that the number of AE hits is proportional to the number of cracks. Consequently, tensile cracks accounted for 78% of the total micro-cracks during the three-point bending tests, which is in accord with the results of Liu et al. (2015). Note that only two kinds of cracks, i.e., tensile crack and shear crack, were assumed in the present study.

To avoid confusion about determining the ratio between the number of AE hits and the number of micro-cracks, AE hits during the rockburst were normalized. Consequently, the evolution process of tensile crack and shear crack can be quantitatively investigated. Due to the space limitations, only some results are given for illustrating the cracking process (see Fig. 16). All specimens seemly experienced a similar cracking process, i.e., tensile cracking occurred first and continued to propagate with a stable manner until shear cracking initiated, and micro-cracks, including tensile and shear cracks, began to localize and developed in an unstable manner until failure occurred. Even after the shear cracks are generated, the growth rate of tensile cracks is still faster than that of shear cracks.

The last ratio of tensile cracks to shear cracks ( $T/S$ ) after test was calculated, and the results are presented in Table 4. As a result, the number of tensile cracks can reach several times than that of shear cracks, and the use of bolt significantly changes the microscopic cracking mechanism. The ratio was significantly reduced due to the use of bolt, and it continues to decrease with the decreasing bolt spacing (Table 4). For specimen M1,  $T/S$  is approximately 7.77. However, when bolt spacing is 140, 100 and 80 mm (specimens M4,

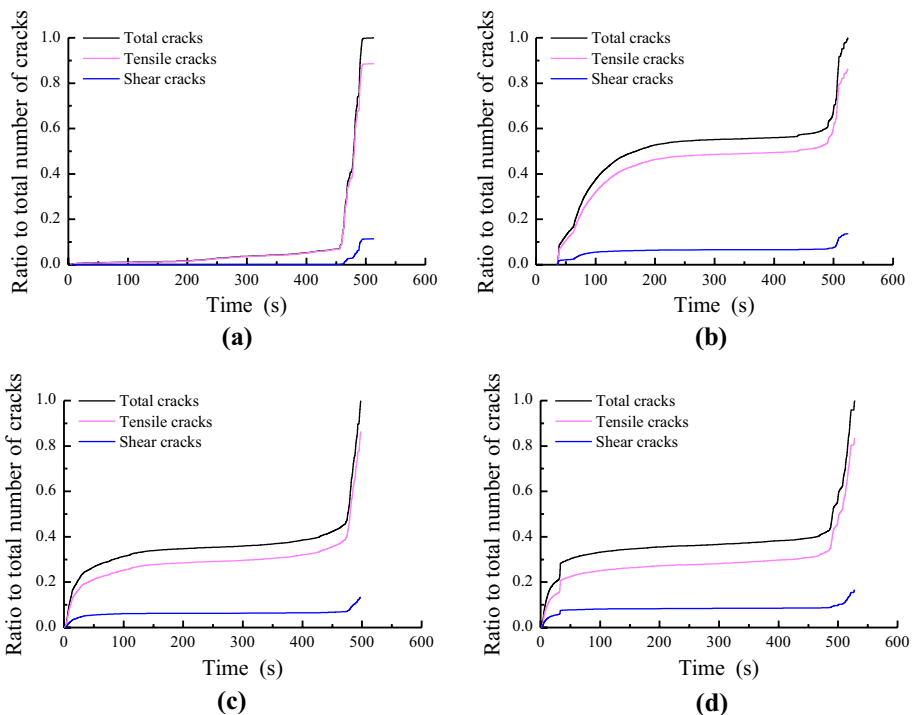


**Fig. 16** Cracking process for specimens: **a** M1; **b** M3; **c** M5; **d** M8. For specimens M3, M5 and M8, shear failure began to occur at approximately 500 s



**Table 4** Ratio between tensile cracks and shear cracks

Sample no.	M1	M2	M3	M4	M5	M6	M7	M8
Bolt spacing (mm)			140	140	100	100	80	80
<i>T/S</i>	7.77	–	6.25	6.79	6.41	6.43	–	5.05

– No information is available

M6 and M8), the ratio decreases to 6.79, 6.43 and 5.05 (Table 4), respectively. In general, bolting-induced confining pressure will be conducive to the occurrence of shear component. Therefore, the trend of monotonic decrease for the *T/S* ratio (Table 4) suggests that bolt effectively restrains the tensile cracking, and the shear component increases with the use of bolt and it continues to increase with decreasing bolt spacing.

### 5 Discussion

It is generally realized that tensile cracks first occurred and continued to propagate with a stable manner (Brace et al. 1966; Lajtai et al. 1990), and it has also been reflected in Fig. 16. Under unconfined or confined compression conditions, coalescence of tensile cracks is considered to be consistent with the initiation of shear fracture (Martin and Chandler 1994; Hajiabdolmajid et al. 2002). In the present study, universal discrete element code UDEC (ITASCA Consulting Group Inc. 2011), in which the number of tensile cracks and shear cracks can be traced, was also used to help to elucidate the relationship between shear fracturing and coalescence of micro-cracks. Figure 17 presents the two numerical simulation results (the size of numerical specimen is 100 mm×200 mm). As expected, we can clearly observe that the initiation of volumetric strain reverse or coalescence is consistent with the initiation of shearing.

As presented in Fig. 16, shearing of laboratory specimens did not initiate until stress level of approximately 0.89 or more of the peak strength was reached (approximately 500 s, and the initial shear cracks are not considered in the present study). From the above analysis, the initiation of shear failure identified by AF/RA (Fig. 16) should correspond to the initiation of

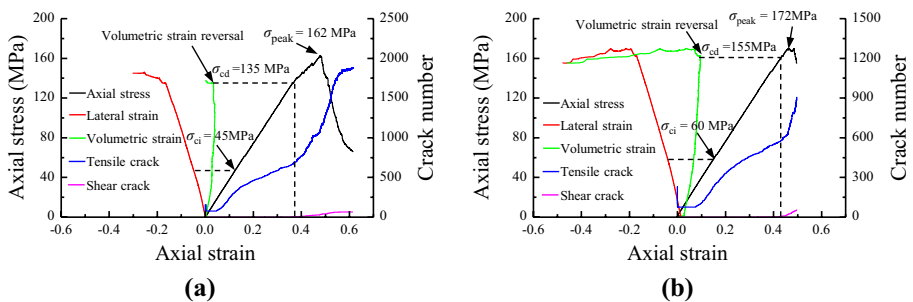


**Fig. 17** Discrete element simulation utilizing bonded-polygon analogy for granite: **a** uniaxial compression test; **b** biaxial compression test with a lateral confining stress = 5 MPa. The ratios between the tensile and shear cracks are 28.45 and 16.54, respectively. Note that the axial stress for initial change in the slope of the lateral strain vs axial stress is identified as  $\sigma_{ci}$ , and the axial stress at reversal in the total volumetric strain curve is identified as  $\sigma_{cd}$

**Table 5** Estimated threshold of  $\sigma_{cd}'$  from cracking process (Fig. 16) identified with AF/RA method

Sample no.	M1	M2	M3	M4	M5	M6	M7	M8
$\sigma_{cd}'/\sigma_{peak}$	0.89	–	0.94	0.94	0.96	0.93	–	0.93

coalescence of cracks or crack damage stress  $\sigma_{cd}$  identified with cumulative AE hits (Fig. 12 or Table 3). Therefore, the stress for shear fracturing in Fig. 16, called  $\sigma_{cd}'$ , is obtained, and its ratios to  $\sigma_{peak}$  are presented in Table 5. As a result,  $\sigma_{cd}'/\sigma_{peak}$  in Table 5 shows a good consistency with  $\sigma_{cd}/\sigma_{peak}$  as presented in Table 3, indicating that it is feasible to quantify the cracking mechanism using AE signals. The value of AF/RA and its resulting quantitative cracking mechanisms under differ bolting conditions are reasonable.

Noted that the ratio of AF/RA is related to the AE transducers, because different types of transducers have different frequency ranges, and this range affects the value of AF as well as AF/RA. Therefore, that the ratio of AF/RA is 1 may only be reasonable if the same rock materials and AE transducer used are used. Another point that needs to be pointed out is that there are few quantitative studies on tensile cracks and shear cracks in the three-point bending test of granite material. The present study can only refer to a small amount of literature and believes that tensile cracks occupy most (approximately 78%) of the micro-cracks in three-point bending test of granite material. The quantitative study of tensile cracks and shear cracks in the three-point bending tests needs further research, which will help distinguish the AE information of tensile cracks and shear cracks.

## 6 Conclusions

Strainburst is one of the most common geological disasters, and considerable efforts had been devoted to understand it. Although bolt support was widely used to prevent the occurrence of rockburst, this violent failure is still frequent. Few studies have investigated the rockburst process and mechanisms under bolt support conditions. In the present study, a representative rock element was introduced and tested with a true-triaxial loading stress path, maintaining one free face while loading on the other five faces, to reproduce in situ rockburst due to compressive stress concentration. Based on high-speed cameras and AE system, the ejection failure process, failure intensity, characteristic stresses, failure mode and cracking mechanisms were investigated in detail. The main observations and conclusions are as follows:

1. Rockburst process under bolt support conditions is composed of grains ejection, splitting into plates, buckling to the point of rupture, and fragments ejection. However, the use of bolt significantly affects the ejection failure. When bolt spacing is large, the rockburst occurs in a weak area in the form of a localized damage after the bolt support; when the bolt spacing is reduced to a certain extent, the weak area will no longer be obvious and rockburst will pass through the bolt and even occur throughout the free face due to strong bolting effect. In addition, the maximum depth of the rockburst pit and the mass of the fragments are reduced with the use of bolt and decreasing bolt spacing. Therefore, the bolt plays an important role in the design of bolting in deep tunnels.
2. Rockburst under the bolt support conditions is more intense, but the intensity decreases with the decreasing bolt spacing under the bolt support condition. In any case, the rockburst possibility under bolt support should be given enough attention, because it may release more energy due to the role of bolt.

3. It was found that the with the use of bolt and the decrease in bolt spacing, crack initiation stress, crack damage stress and peak strength increased and the cracking activities was retarded.
4. Macroscopic failure mode and microscopic cracking mechanism under bolt support are significantly different from that without bolt. With the use of bolt, tensile splitting becomes less obvious near the free face. Further, the tensile splitting continues to weaken with the decreasing bolt spacing. In addition, quantitative results based on ratio AF/RA show that the ratio between tensile cracks and shear cracks is lower with the use bolt, and it continues to decrease with the decreasing bolt spacing (i.e., shear cracking component gradually increases with the decreasing bolt spacing).

It should be noted that the bolt used in the present study is only a substitute of a real bolt, and the mechanics similarity and geometric similarity of bolt need further research. But we also believe that the results provide meaningful insights into rockburst characteristics and mechanisms under bolt support conditions. In addition, we should also strengthen the study of in situ rockburst under the conditions of bolt support.

**Acknowledgements** The authors would like to thank for the support from the National Natural Science Foundation of China under Grant No. 41472329. The work in this paper was also supported by the Opening Fund of State Key Laboratory of Geohazard Prevention and Geoenvironment Protection (Chengdu University of Technology) under Grant No. SKLGP2017K022, Institute of Rock and Soil Mechanics, Chinese Academy of Sciences under Grant No. Z016009, the Guangxi Natural Science Foundation under Grant No. 2016GXNSFGA380008 and the Innovation Project of Guangxi Graduate Education under Grant No. YCBZ2018025.

## References

- Aggelis DG (2011) Classification of cracking mode in concrete by acoustic emission parameters. *Mech Res Commun* 38(3):153–157
- Brace WF, Paulding BW, Scholz C (1966) Dilatancy in the fracture of crystalline rocks. *J Geophys Res* 71(16):3939–3953
- Cai M, Kaiser PK (2014) In-situ rock spalling strength near excavation boundaries. *Rock Mech Rock Eng* 47(2):659–675
- Chang C, Haimson B (2000) True triaxial strength and deformability of the German Continental Deep Drilling Program (KTB) deep hole amphibolite. *J Geophys Res-Sol Earth* 105(B8):18999–19013
- Chen WZ, Lu SP, Guo XH, Qiao CJ (2009) Research on unloading confining pressure tests and rockburst criterion based on energy theory. *Chin J Rock Mech Eng* 28(8):1530–1540 (in Chinese)
- Cheon DS, Jeon S, Chan P, Song WK, Park ES (2011) Characterization of brittle failure using physical model experiments under polyaxial stress conditions. *Int J Rock Mech Min* 48(1):152–160
- Cook NGW (1963) The basic mechanics of rockbursts. *J S Afr Inst Min Metall* 64(3):71–81
- Cook NGW (1965) The failure of rock. *Int J Rock Mech Min Sci Geomech Abstr* 2(4):389–403
- Cook NGW, Hoek E, Pretorius JP, Ortlepp WD, Salamon MDG (1966) Rock mechanics applied to study of rockbursts. *J S Afr Inst Min Metall* 66(10):435–528
- Diederichs MS (2007) The 2003 Canadian geotechnical colloquium: mechanistic interpretation and practical application of damage and spalling prediction criteria for deep tunnelling. *Can Geotech J* 44(9):1082–1116
- Feng XT, Chen BR, Zhang CQ, Li SJ, Wu SY (2013) Mechanism, warning and dynamic control of rockburst development processes. China Social Sciences Publishing House, Beijing
- Feng XT, Yu Y, Feng GL, Xiao YX, Chen BR, Jiang Q (2016) Fractal behaviour of the microseismic energy associated with immediate rockbursts in deep, hard rock tunnels. *Tunn Undergr Space Technol* 51:98–107

- Gao FQ, Kaiser PK, Stead D, Eberhardt E, Elmo D (2019) Strainburst phenomena and numerical simulation of self-initiated brittle rock failure. *Int J Rock Mech Min* 116:52–63. <https://doi.org/10.1016/j.ijrmm.2019.03.021>
- Gong W, Peng Y, Wang H, He M, Sousa LRE, Wang J (2015) Fracture angle analysis of rock burst faulting planes based on true-triaxial experiment. *Rock Mech Rock Eng* 48(3):1017–1039
- Gong FQ, Luo Y, Li XB, Si XF, Tao M (2018) Experimental simulation investigation on rockburst induced by spalling failure in deep circular tunnels. *Tunn Undergr Space Technol* 81:413–427
- Gong FQ, Si XF, Li XB, Wang SY (2019) Experimental investigation of strain rockburst in circular caverns under deep three-dimensional high-stress conditions. *Rock Mech Rock Eng* 52(5):1459–1474
- Grosse CU, Ohtsu M (2008) *Acoustic emission testing*. Springer, Berlin
- Hajiabdolmajid V, Kaiser PK, Martin CD (2002) Modelling brittle failure of rock. *Int J Rock Mech Min* 39(6):731–741
- He MC, Miao JL, Feng JL (2010) Rock burst process of limestone and its acoustic emission characteristics under true-triaxial unloading conditions. *Int J Rock Mech Min* 47(2):286–298
- He MC, Jia XN, Coli M, Livi E, Luis S (2012) Experimental study of rockbursts in underground quarrying of Carrara marble. *Int J Rock Mech Min* 52:1–8
- Hedley DG (1992) *Rockburst handbook for Ontario hardrock mines*. Canmet, Ottawa
- Hua AZ, You MQ (2001) Rock failure due to energy release during unloading and application to underground rock burst control. *Tunn Undergr Space Technol* 16(3):241–246
- Kaiser PK (1996) *Canadian rockburst support handbook: 1996*. Geomechanics Research Centre
- Kaiser PK, Cai M (2012) Design of rock support system under rockburst condition. *J Rock Mech Geotech Eng* 04(3):215–227
- Kaiser PK, Diederichs MS, Martin CD, Sharp J, Steiner W (2000) Underground works in hard rock tunneling and mining. In: *ISRM international symposium*
- Lajtai EZ, Carter BJ, Ayari ML (1990) Criteria for brittle fracture in compression. *Eng Fract Mech* 37(1):59–74
- Liu JP, Liu ZS, Wang SQ, Li YH (2015) Analysis of acoustic emission source mechanisms for tensile and shear cracks of rock fractures. *J Northeast Univ* 36(11):1624–1628
- Martin CD (1997) Seventeenth Canadian geotechnical colloquium: the effect of cohesion loss and stress path on brittle rock strength. *Can Geotech J* 34(5):698–725
- Martin CD, Chandler NA (1994) The progressive fracture of Lac du Bonnet granite. *Int J Rock Mech Min Sci Geomech Abstr* 31(6):643–659
- Martin CD, Christiansson R (2009) Estimating the potential for spalling around a deep nuclear waste repository in crystalline rock. *Int J Rock Mech Min* 46(2):219–228
- Ortlepp WD (2000) Observation of mining-induced faults in an intact rock mass at depth. *Int J Rock Mech Min* 37(1–2):423–436
- Ortlepp W, Stacey T (1994) Rockburst mechanisms in tunnels and shafts. *Tunn Undergr Space Technol* 9(1):59–65
- Salamon MDG (1970) Stability, instability and design of pillar workings. *Int J Rock Mech Min Sci Geomech Abstr* 7(6):613–631
- Shahidan S, Pulin R, Bunnori NM, Holford KM (2013) Damage classification in reinforced concrete beam by acoustic emission signal analysis. *Constr Build Mater* 45(13):78–86
- Singh SP (1987) The influence of rock properties on the occurrence and control of rockbursts. *Min Sci Technol* 5(1):11–18
- Su GS, Jiang JQ, Zhai SB, Zhang GL (2017a) Influence of tunnel axis stress on strainburst: an experimental study. *Rock Mech Rock Eng* 50(10):1551–1567
- Su GS, Zhai SB, Jiang JQ, Zhang GL, Yan LB (2017b) Influence of radial stress gradient on strainbursts: an experimental study. *Rock Mech Rock Eng* 50(10):2659–2676
- Tang CA, Wang JM, Zhang JJ (2010) Preliminary engineering application of microseismic monitoring technique to rockburst prediction in tunneling of Jinping II project. *J Rock Mech Geotech Eng* 2(3):193–208
- Wang JM, Zeng XH, Zhou JF (2012) Practices on rockburst prevention and control in headrace tunnels of Jinping II hydropower station. *J Rock Mech Geotech Eng* 4(3):258–268
- Weng L, Li X, Taheri A, Wu Q, Xie X (2018) Fracture evolution around a cavity in brittle rock under uniaxial compression and coupled static-dynamic loads. *Rock Mech Rock Eng* 51(2):1–15
- Zhang XJ (2011) Experimental research on splitting rock burst of surrounding rocks in deep roadways (tunnels). *J Min Saf Eng* 28(1):66–71
- Zhang CQ, Feng XT, Zhou H, Qiu SL, Wu WP (2012) Case histories of four extremely intense rockbursts in deep tunnels. *Rock Mech Rock Eng* 45(3):275–288

- Zhang CQ, Feng XT, Zhou H, Qiu SL, Wu WP (2013) Rockmass damage development following two extremely intense rockbursts in deep tunnels at Jinping II hydropower station, southwestern China. *Bull Eng Geol Environ* 72(2):237–247
- Zhang CQ, Feng XT, Zhou H, Qiu SL, Yang YS (2014) Rock mass damage induced by rockbursts occurring on tunnel floors: a case study of two tunnels at the Jinping II Hydropower Station. *Environ Earth Sci* 71(1):441–450
- Zhao XG, Cai M (2014) Influence of specimen height-to-width ratio on the strainburst characteristics of Tianhu granite under true-triaxial unloading conditions. *Can Geotech J* 52(7):890–902
- Zhao XG, Wang J, Cai M, Cheng C, Ma LK, Su R, Zhao F, Li DJ (2014) Influence of unloading rate on the strainburst characteristics of Beishan granite under true-triaxial unloading conditions. *Rock Mech Rock Eng* 47(2):467–483
- Zhu TT, Jing HW, Hai-Jian SU, Qian Y, Ming-Rui DU (2015) Mechanical behavior of sandstone containing double circular cavities under uniaxial compression. *Chin J Geotech Eng* 37(6):1047–1056 (**in Chinese**)
- Zuo YJ, Li XB, Tang CA, Zhang YP, Ma CD, Yan CB (2006) Experimental investigation on failure of rock subjected to 2 D dynamic-static coupling loading. *Chin J Rock Mech Eng* 25(9):1809–1820 (**in Chinese**)

**Publisher's Note** Springer Nature remains neutral with regard to jurisdictional claims in published maps and institutional affiliations.